




Decomposing large unitaries into multimode devices of arbitrary size

Christian Arends ^{1,2}, Lasse Wolf ³, Jasmin Meinecke,^{4,5,6,7} Sonja Barkhofen,^{2,8} Tobias Weich ^{3,2} and Tim J. Bartley^{2,8}¹Department of Mathematics, Aarhus University, Ny Munkegade 118, 8000 Aarhus C, Denmark²PhoQS, Universität Paderborn, Warburger Strasse 100, 33098 Paderborn, Germany³Institute of Mathematics, Universität Paderborn, Warburger Strasse 100, 33098 Paderborn, Germany⁴Max-Planck-Institut für Quantenoptik, 85748 Garching, Germany⁵Department für Physik, Ludwig-Maximilians-Universität, 80539 München, Germany⁶Munich Center for Quantum Science and Technology (MCQST), 80799 München, Germany⁷Institute of Solid State Physics, Technische Universität Berlin, 10623 Berlin, Germany⁸Department of Physics, Universität Paderborn, Warburger Strasse 100, 33098 Paderborn, Germany

(Received 29 September 2023; accepted 23 January 2024; published 29 February 2024)

Decomposing complex unitary evolution into a series of constituent components is a cornerstone of practical quantum information processing. While the decomposition of an $n \times n$ unitary into a product of 2×2 subunitaries (which can for example be realized by beam splitters and phase shifters in linear optics) is well established, we show how for any $m > 2$ this decomposition can be generalized into a product of $m \times m$ subunitaries (which can then be realized by a more complex device acting on m modes). If the cost associated with building each $m \times m$ multimode device is less than constructing with $\frac{m(m-1)}{2}$ individual 2×2 devices, we show that the decomposition of large unitaries into $m \times m$ submatrices is more resource efficient and exhibits a higher tolerance to errors, than its 2×2 counterpart. This allows larger-scale unitaries to be constructed with lower errors, which is necessary for various tasks, not least boson sampling, the quantum Fourier transform, and quantum simulations.

DOI: [10.1103/PhysRevResearch.6.L012043](https://doi.org/10.1103/PhysRevResearch.6.L012043)

Unitary transformations of modes [1] are the basis of quantum information processing and quantum simulation. While transformations on a small number of modes are relatively straightforward, many algorithms and applications require the implementation of joint unitary transformations on a large number of modes; pertinent examples include boson sampling [2,3], the quantum Fourier transform [4,5], quantum photonic simulation [6], and, outside of quantum photonics, neuromorphic computing [7]. Typically these large $n \times n$ unitaries are constructed from a decomposition into a collection of smaller 2×2 unitaries. While this approach is used independent of the physical platform (see, e.g., Ref. [8]), it is very common in linear optics where 2×2 transformations can be easily implemented by beam splitters and phase shifters, the established building blocks of linear optics. In their seminal paper, Reck *et al.* demonstrated how to mathematically decompose any $n \times n$ unitary in a product of $n(n-1)/2$ 2×2 subunitaries. Their decomposition results in a triangular array of beam splitters and phase shifters, which can be programmed to implement an arbitrary linear transform of optical modes [9]. This scheme has been refined by Clements *et al.* enhancing the loss tolerance using a symmetric arrangement of 2×2 splitters

[10]. Furthermore, the length of the circuit could be shortened with symmetric 2×2 splitters [11]. Indeed, with the advent of integrated optics, in which many beam splitters and phase shifters can be implemented on a small footprint, large and complex unitary operations have been demonstrated using this approach, not least linear optics quantum computing [12–14], boson sampling [15–17], quantum simulation [18–20], and neuromorphic computing [21,22]. Nevertheless, while sources and detectors scale linearly with the network dimension n , the required number of beam splitters and phase shifters scales with $O(n^2)$, in order to implement an arbitrary $n \times n$ unitary. It is therefore pertinent to investigate building large unitaries starting from larger building blocks.

Beyond decompositions of large unitaries into arrays of beam splitters, other approaches such as multiport integrated devices and 3×3 fiber tritters have also been investigated [23] in the context of quantum interference [24–27]. Higher-order modal manipulation of quantum light has also been investigated beyond the spatial degree of freedom, which is highly promising for experimentally implementing unitaries of larger size. For example, methods for manipulating orbital angular momentum modes have been shown up to seven modes [28], however, generalized manipulation remains challenging [29]. In the frequency degree of freedom, operations on ten modes have been shown [30], while operations on hybrid time-frequency modes have also been demonstrated up to 64 modes [31–34]. This begs the question: How can larger $n \times n$ unitaries be constructed from $m \times m$ constituent unitaries, where $m > 2$?

Published by the American Physical Society under the terms of the [Creative Commons Attribution 4.0 International](https://creativecommons.org/licenses/by/4.0/) license. Further distribution of this work must maintain attribution to the author(s) and the published article's title, journal citation, and DOI.

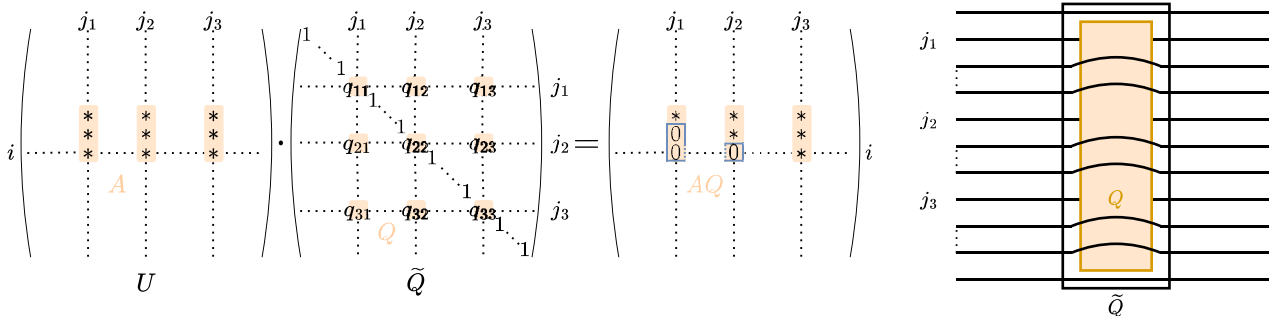


FIG. 1. Example of the matrix embedding for $m = 3$ (left). The matrix \tilde{Q} only affects the input modes j_1, \dots, j_m . This is illustrated on the circuit diagram (right).

The answer to this question becomes practically relevant only when the $m \times m$ constituent device outperforms (by some reasonable metric) its own decomposition into 2×2 components. In other words, if the performance cost (e.g., loss, fidelity, production cost, etc.) associated with producing an $m \times m$ unitary is greater than the $\frac{m(m-1)}{2}$ different 2×2 unitaries, the 2×2 decomposition is more efficient. Nevertheless, once it becomes cheaper to directly fabricate a device realizing an $m \times m$ unitary compared to building it out of 2×2 phase-shifter/beam-splitter cascades, the question how one can efficiently build an $n \times n$ unitary from its $m \times m$ subunitaries is of the utmost relevance. Indeed, in all the aforementioned physical implementations, the number of possible modes is physically restricted far below the desired matrix size for quantum computing applications.

In this Letter, we generalize unitary decomposition of an $n \times n$ unitary into $m \times m$ submatrices, where $n > m \geq 2$. This provides a significant scaling advantage whenever it is cheaper to produce an $m \times m$ unitary directly, compared to building it out of 2×2 unitaries. We provide an algorithmic approach to find this decomposition, which uses the best-known minimum number of submatrices. We also show that quality thresholds exist when comparing larger devices to the established beam-splitter decomposition. This provides a route to implementing large-scale devices, which, by reducing the total number of components, are more tolerant to the errors caused by the components individually.

The algorithm to decompose a unitary $n \times n$ matrix U into a product of smaller unitary matrices of dimension $m \times m$ runs as follows: The key task is to find $m \times m$ matrices $\tilde{Q}_1, \dots, \tilde{Q}_N$ (properly embedded as $n \times n$ matrices) such that $U\tilde{Q}_1 \dots \tilde{Q}_N$ is an upper triangular matrix. Note that any unitary upper triangular matrix is automatically a diagonal unitary matrix D . Such diagonal matrices are experimentally easy to realize because they consist only of a phase shift in each individual mode. Summarizing, our algorithm will allow to write the large unitary U as $U = D\tilde{Q}_N^{-1} \dots \tilde{Q}_1^{-1}$, thus we have factorized U into $m \times m$ unitaries and final phase shifts.

In order to achieve upper triangular matrices we use the RQ decomposition which, for any $m \times m$ matrix A , ensures the existence of a unitary matrix Q and an upper triangular matrix R (i.e., $R_{ij} = 0$ for $i > j$) such that $A = RQ^{-1}$ (see, e.g., Sec. 5.2 in Ref. [35]). In particular, AQ is upper triangular

so that we can transform any matrix into an upper triangular one by right multiplication with a unitary.

We now describe how to use the RQ decomposition to create zeros at predefined positions in a large unitary matrix U . We will use this multiple times to create zeros at all places below the diagonal. Let us fix m columns $1 \leq j_1 < \dots < j_m \leq n$ and a base row $i \in \{m, \dots, n\}$. This choice gives rise to an $m \times m$ matrix A consisting of the entries of U which are contained in the columns j_1, \dots, j_m and in the rows $i - m + 1, \dots, i$ (see Fig. 1 for an illustration of this embedding for $m = 3$). Our goal is to transform this matrix into an upper triangular form. First, by the RQ decomposition, there is a unitary matrix Q such that $AQ = R$ is upper triangular. We now show how to properly embed the matrix Q into an $(n \times n)$ matrix such that we can create zeros in our original matrix U . For this let q_{kl} denote the entries of the $m \times m$ matrix Q and build an $n \times n$ matrix \tilde{Q} with entries \tilde{q}_{kl} as follows: Start with the identity matrix and set $\tilde{q}_{j_k, j_l} := q_{kl}$, i.e., we embed Q into the identity matrix at the $m \times m$ submatrix given by the entries having their row and column coordinates both in $\{j_1, \dots, j_m\}$. Thus, $U\tilde{Q}$ has an upper triangular $m \times m$ submatrix. More precisely, the entries in row l and column j_k are zero for $l = i - m + 1 + k, \dots, i$ and $k = 1, \dots, m$. Note that the multiplication with \tilde{Q} from the right only affects the columns j_1, \dots, j_m of U . Moreover, if there are only zeros in these columns below the i th row, all these zeros are maintained by this multiplication. To state this differently, if U has zeros at (l, j_k) , $k = 1, \dots, m$, this is equivalent to saying that an input state that occupies only the modes j_1, \dots, j_m is transformed to an output state where the l th mode is not occupied. Since \tilde{Q} only affects the input modes j_1, \dots, j_m , this property is preserved if we apply the matrix \tilde{Q} before applying U , which means that we consider $U\tilde{Q}$.

The algorithm to find the matrices Q_i we are presenting works similarly to a Tetris game: In each step we create zeros in a specific row by inserting blocks of zeros using the technique previously described. If $m = 2$ then this algorithm is exactly the algorithm of Ref. [9]. We start by creating zeros in the bottom row. By selecting the first m columns and using the RQ decomposition as above, we can build an upper triangular $m \times m$ block in the lower left corner of U (see Fig. 2). This gives us the matrix \tilde{Q}_1 . We now proceed in the same way with the next m columns without zero entries to create more and more triangle-shaped blocks of zeros in that row until

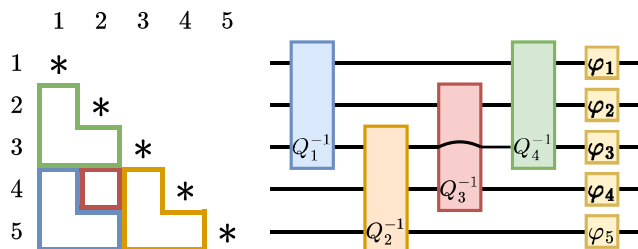


FIG. 2. Decomposition for $m = 3$ and $n = 5$ (left) with an experimental circuit (right). In a first step we can create an upper triangular matrix in the lower left 3×3 submatrix, which means that we produce zeros on the blue L-shaped region. In the next step the submatrix Q_2^{-1} creates zeros in the yellow L-shaped region. This operation is followed by a two-mode device that only acts on modes 2 and 4 and creates a zero in the red box. Finally, the submatrix Q_4^{-1} creates further zeros in the green L-shaped region. The final phase shifts $\varphi_1, \dots, \varphi_5$ transform the matrix to the identity matrix. Continuous lines that bypass a colored box in the circuit diagram (e.g., mode 3 in Q_3^{-1}) denote modes that are not affected by the submatrix operation.

the number m' of remaining nonzero entries is less than m and use (potentially) one more matrix of size m' to fill in the remaining zeros—a triangle-shaped block of size m' . As we already created some zeros in the penultimate row, we only have to create new zeros at the places which are not already covered. Here, we have to split up the triangle-shaped block and use selected columns j_1, \dots, j_m as described above. In general, the algorithm is structured as follows:

(1) Let $i \in \{2, \dots, n\}$ be the smallest value such that in the rows $i + 1, \dots, n$ all entries below the diagonal are zero. In the first step described above we generically have no zeros in the last row, i.e., $i = n$.

(2) Consider the i th row and pick the first m nonzero entries in that row which are on the left-hand side of the diagonal or on the diagonal. Denote the corresponding columns by j_1, \dots, j_m . If there are just $2 \leq m' < m$ nonzero entries left in that row, proceed with m' instead of m .

(3) Choose a unitary matrix corresponding to the row i and the columns j_1, \dots, j_m to create an upper triangular block of size m , as described above.

(4) Repeat until U is transformed into an upper triangular matrix. Figures 2 and 3 show illustrations of the decomposition, exemplary for a 5×5 and a 13×13 unitary, respectively, together with the corresponding physical network.

Each $m \times m$ submatrix \tilde{Q}_i creates $\frac{1}{2}(m - 1)m$ zeros in the matrix U . In total we have to create $\frac{1}{2}(n - 1)n$ zeros to end up with a diagonal matrix. Hence, we need at most $\frac{n(n-1)}{m(m-1)}$ matrices \tilde{Q}_i which come from an $m \times m$ matrix. In addition, our algorithm requires at most one $m' \times m'$ submatrix with $m' < m$ for each row. Hence, we end up with at most $\frac{n(n-1)}{m(m-1)} + n - 1$ matrices \tilde{Q}_i (see Fig. 4).

If c_m is the relevant cost of an $m \times m$ unitary, then the total cost for constructing the $n \times n$ matrix out of $m \times m$ matrices is $C_{n,m} \leq c_m(\frac{n(n-1)}{m(m-1)} + n - 1)$ (under the assumption that the total cost is linear in the number of utilized

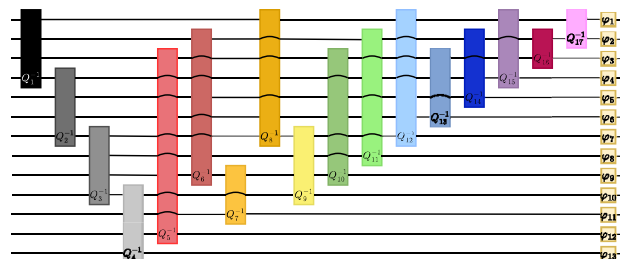
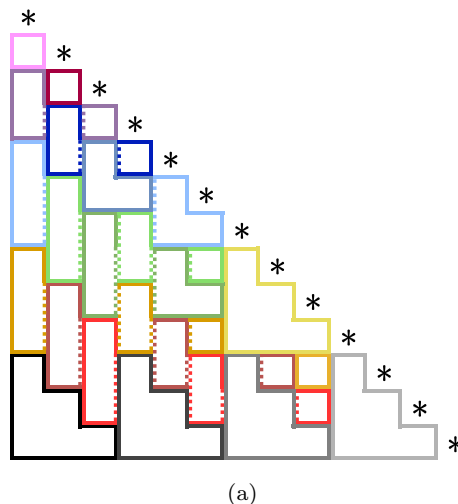


FIG. 3. (a) Illustration of the algorithm using triangle blocks for $m = 4$ and $n = 13$ and (b) corresponding circuit diagram. Each colored region corresponds to the zeros created by the action of one multimode device. Note that in the last line all four-mode devices act on adjacent modes and thus the colored regions are connected step-shaped regions. By contrast, the red region in the penultimate line is split over modes 3, 6 and 9, which is possible due to a matrix embedding as described in Fig. 1. Note that as in the example presented in Fig. 2, at some places one may also use subunitaries of smaller size, e.g., the pink box on the top that stems from a 2×2 unitary.

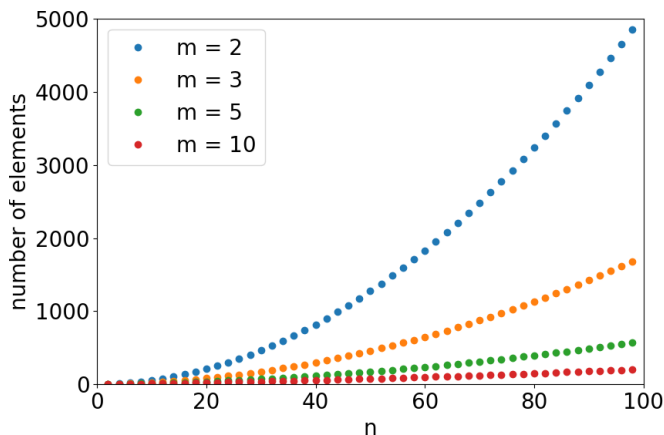


FIG. 4. Scaling behavior of our algorithm for the number of elements to construct a unitary of size n according to $\frac{n(n-1)}{m(m-1)} + n - 1$.

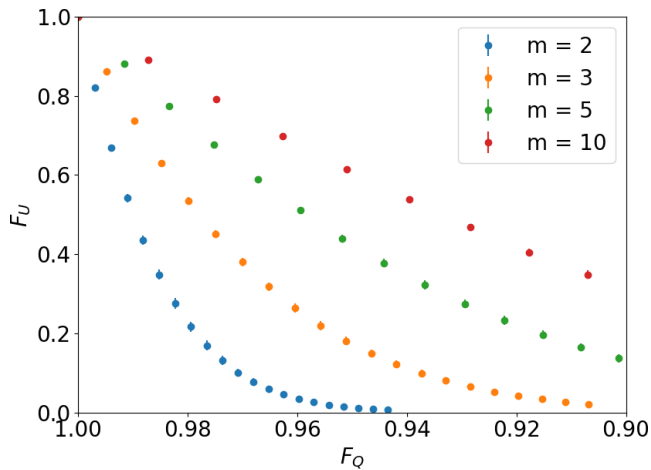


FIG. 5. Numerical simulations of the fidelity for $n = 50$. For each data point we reconstructed 100 random unitary matrices U , each with 20 different perturbations and averaged over all 2000 reconstructions. The size of the calculated submatrices is indicated in the legend. The error bars of the statistical fluctuations are smaller than the symbol size.

devices). Recall that the Reck or Clements scheme requires $\frac{1}{2}n(n-1)$ different 2×2 unitaries which leads to a relevant cost of $C_{n,2} = \frac{c_2}{2}n(n-1)$ for the realization of a 2×2 unitary. Comparing these two cost functions one sees directly that whenever $c_m < \frac{1}{2}m(m-1)$ (i.e., the $m \times m$ device is cheaper than building the matrix out of 2×2 matrices), one sees that for large n , $C_{n,m} < C_{n,2}$, i.e., it is advantageous to build the $n \times n$ matrix out of $m \times m$ instead of the traditional 2×2 beam-splitter/phase-shifter cascades.

We numerically implemented the above described algorithm in order to test its performance as well as its robustness against perturbations: For this, we randomly chose a $n \times n$ unitary matrix U and decomposed it into $m \times m$ unitaries Q_i as described above. We then perturbed the calculated $m \times m$ submatrices Q_i by adding random numbers from a normal distribution with specified width (“noise strength”) to the real and imaginary part of the entries, respectively. As a figure of merit for the strength of the perturbation we consider the fidelity of the perturbed submatrices Q_{pert} and the original submatrices Q [10] given by

$$F(Q, Q_{\text{pert}}) := \left| \frac{\frac{1}{m} \text{Tr}(Q^\dagger \cdot Q_{\text{pert}})}{\sqrt{\frac{1}{m} \text{Tr}(Q_{\text{pert}}^\dagger \cdot Q_{\text{pert}})}} \right|^2. \quad (1)$$

This will of course vary for any realized perturbation so we take the expected reconstruction fidelity $F_Q := \mathbb{E}[F(Q, Q_{\text{pert}})]$ as a measure for the precision of our individual components Q . Next, we reconstruct a $(n \times n)$ -matrix U_{pert} from the Q_{pert} . The final metric to analyze the robustness of U is defined by $F(U, U_{\text{pert}})$ respectively by the expected fidelity $F_U := \mathbb{E}[F(U, U_{\text{pert}})]$ and plotted in Figs. 5 and 6. In the first figure, we fixed the matrix size at $n = 50$ and plot the dependence of the reconstruction fidelity F_U as a function of the component quality F_Q for different submatrix sizes $m = 2, 3, 5, 10$. It can be clearly seen from the figure that the reconstruction fidelity of F_U drops quickly with component quality F_Q . The smaller

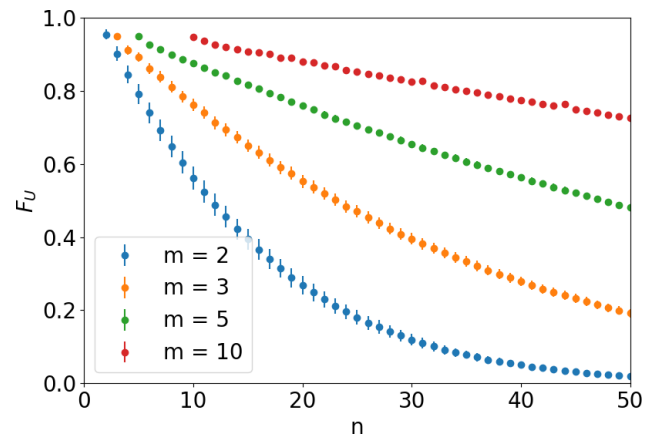


FIG. 6. Numerical simulations of the fidelity for increasing $n \geq m$ at a fixed component quality $F_Q = 0.95 \pm 0.0005$. For each data point we reconstructed 100 random unitary matrices U , each with 20 different perturbations. The size of the submatrices is indicated in the legend. The error bars of the statistical fluctuations are often smaller than the symbol size.

the submatrices are (i.e., the smaller m), the steeper is the fidelity drop. Thus, already the increase in component size from $m = 2$ to $m = 3$ improves significantly the fidelity of the final unitary and proves a much higher robustness of the reconstructed matrix U_{pert} . Second, we analyzed the question of how big the final system size (i.e., unitary size n) can become, given components of size m achieving a specified quality F_Q . The results for a fixed value $F_Q = 0.95 \pm 0.0005$ and $m = 2, 3, 5, 10$ are presented in Fig. 6. Again, we observe already for $m = 3$ a significant advancement in fidelity which enables the realization of much bigger matrices, i.e., quantum networks, at reasonable fidelities. The advantage increases with the size of the submatrices, as expected. Of course it should be noted that Fig. 6 compares m -mode devices of increasing size m , assuming that the fidelity for each individual device is the same, independent of m . In practice one expects the fidelity to decrease for more complex devices, so again there is an obvious competition between the increasing challenge to construct accurate m -mode devices and the benefit that comes from a more efficient decomposition of large unitaries.

In conclusion, we have presented an algorithm to decompose large $n \times n$ unitaries into smaller constituent $m \times m$ subunitaries. We have shown that these become more tolerant to loss and errors as m increases, yielding the intuition that larger unitaries are more effectively building from larger building blocks. This has implications for building large-scale unitary dynamics on quantum systems, in particular linear optics, where the decomposition in terms of 2×2 beam splitters and phase shifters has become ubiquitous. Exploring other devices which intrinsically operate on a larger set of modes simultaneously is thus highly advantageous, and may simplify the path towards practical large-scale devices.

This work has received funding from the European Union’s Horizon 2020 research and innovation program under Grant Agreement No. 665148 as well as from Deutsche Forschungs-

gemeinschaft (DFG) Grants No. 422642921 (Emmy Noether group “Microlocal Methods for Hyperbolic Dynamics”) and No. SFB-TRR 358/1 2023 – 491392403 (CRC “Integral Structures in Geometry and Representation Theory”) as well

as funding by the Ministerium für Kultur und Wissenschaft des Landes Nordrhein-Westfalen via the project PhoQC. J.M. acknowledges support by the DFG under Germany’s Excellence Strategy EXC-2111 390814868.

- [1] We use the expression “mode” in the context of optics; mathematically speaking, a mode then corresponds to a one-dimensional subspace of a given Hilbert space and an m -mode device is a linear transformation acting on an m -dimensional subspace.
- [2] S. Aaronson and A. Arkhipov, The computational complexity of linear optics, in *Proceedings of the Forty-Third Annual ACM Symposium on Theory of Computing, STOC '11* (Association for Computing Machinery, New York, 2011), pp. 333–342.
- [3] C. S. Hamilton, R. Kruse, L. Sansoni, S. Barkhofen, C. Silberhorn, and I. Jex, Gaussian boson sampling, *Phys. Rev. Lett.* **119**, 170501 (2017).
- [4] P. W. Shor, Algorithms for quantum computation: Discrete logarithms and factoring, in *Proceedings of the 35th Annual Symposium on Foundations of Computer Science* (IEEE, New York, 1994), pp. 124–134.
- [5] D. Coppersmith, An approximate Fourier transform useful in quantum factoring, [arXiv:quant-ph/0201067](https://arxiv.org/abs/quant-ph/0201067).
- [6] A. Aspuru-Guzik and P. Walther, Photonic quantum simulators, *Nat. Phys.* **8**, 285 (2012).
- [7] B. J. Shastri, A. N. Tait, T. Ferreira de Lima, W. H. P. Pernice, H. Bhaskaran, C. D. Wright, and P. R. Prucnal, Photonics for artificial intelligence and neuromorphic computing, *Nat. Photonics* **15**, 102 (2021).
- [8] V. Ramakrishna, R. Ober, X. Sun, O. Steuernagel, J. Botina, and H. Rabitz, Explicit generation of unitary transformations in a single atom or molecule, *Phys. Rev. A* **61**, 032106 (2000).
- [9] M. Reck, A. Zeilinger, H. J. Bernstein, and P. Bertani, Experimental realization of any discrete unitary operator, *Phys. Rev. Lett.* **73**, 58 (1994).
- [10] W. R. Clements, P. C. Humphreys, B. J. Metcalf, W. S. Kolthammer, and I. A. Walmsley, Optimal design for universal multiport interferometers, *Optica* **3**, 1460 (2016).
- [11] B. A. Bell and I. A. Walmsley, Further compactifying linear optical unitaries, *APL Photonics* **6**, 070804 (2021).
- [12] J. Carolan, C. Harrold, C. Sparrow, E. Martín-López, N. J. Russell, J. W. Silverstone, P. J. Shadbolt, N. Matsuda, M. Oguma, M. Itoh, G. D. Marshall, M. G. Thompson, J. C. F. Matthews, T. Hashimoto, J. L. O’Brien, and A. Laing, Universal linear optics, *Science* **349**, 711 (2015).
- [13] W. Bogaerts, D. Pérez, J. Capmany, D. A. B. Miller, J. Poon, D. Englund, F. Morichetti, and A. Melloni, Programmable photonic circuits, *Nature (London)* **586**, 207 (2020).
- [14] N. C. Harris, D. Bunandar, M. Pant, G. R. Steinbrecher, J. Mower, M. Prabhu, T. Baehr-Jones, M. Hochberg, and D. Englund, Large-scale quantum photonic circuits in silicon, *Nanophotonics* **5**, 456 (2016).
- [15] J. B. Spring, B. J. Metcalf, P. C. Humphreys, W. S. Kolthammer, X.-M. Jin, M. Barbieri, A. Datta, N. Thomas-Peter, N. K. Langford, D. Kundys, J. C. Gates, B. J. Smith, P. G. R. Smith, and I. A. Walmsley, Boson sampling on a photonic chip, *Science* **339**, 798 (2013).
- [16] A. Crespi, R. Osellame, R. Ramponi, D. J. Brod, E. F. Galvão, N. Spagnolo, C. Vitelli, E. Maiorino, P. Mataloni, and F. Sciarrino, Integrated multimode interferometers with arbitrary designs for photonic boson sampling, *Nat. Photonics* **7**, 545 (2013).
- [17] L. S. Madsen, F. Laudenbach, M. F. Askarani, F. Rortais, T. Vincent, J. F. F. Bulmer, F. M. Miatto, L. Neuhaus, L. G. Helt, M. J. Collins, A. E. Lita, T. Gerrits, S. W. Nam, V. D. Vaidya, M. Menotti, I. Dhand, Z. Vernon, N. Quesada, and J. Lavoie, Quantum computational advantage with a programmable photonic processor, *Nature (London)* **606**, 75 (2022).
- [18] C. Sparrow, E. Martín-López, N. Maraviglia, A. Neville, C. Harrold, J. Carolan, Y. N. Joglekar, T. Hashimoto, N. Matsuda, J. L. O’Brien, D. P. Tew, and A. Laing, Simulating the vibrational quantum dynamics of molecules using photonics, *Nature (London)* **557**, 660 (2018).
- [19] R. van der Meer, Z. Huang, M. C. Anguita, D. Qu, P. Hooijschuur, H. Liu, M. Han, J. J. Renema, and L. Cohen, Experimental simulation of loop quantum gravity on a photonic chip, *npj Quantum Inf.* **9**, 32 (2023).
- [20] F. H. B. Somhorst, R. van der Meer, M. Correa Anguita, R. Schadow, H. J. Snijders, M. de Goede, B. Kassenberg, P. Venderbosch, C. Taballione, J. P. Epping, H. H. van den Vlekert, J. Timmerhuis, J. F. F. Bulmer, J. Lugani, I. A. Walmsley, P. W. H. Pinkse, J. Eisert, N. Walk, and J. J. Renema, Quantum simulation of thermodynamics in an integrated quantum photonic processor, *Nat. Commun.* **14**, 3895 (2023).
- [21] J. M. Shainline, S. M. Buckley, R. P. Mirin, and S. W. Nam, Superconducting optoelectronic circuits for neuromorphic computing, *Phys. Rev. Appl.* **7**, 034013 (2017).
- [22] J. Feldmann, N. Youngblood, C. D. Wright, H. Bhaskaran, and W. H. P. Pernice, All-optical spiking neurosynaptic networks with self-learning capabilities, *Nature (London)* **569**, 208 (2019).
- [23] L. B. Soldano and E. C. M. Pennings, Optical multi-mode interference devices based on self-imaging: Principles and applications, *J. Lightwave Technol.* **13**, 615 (1995).
- [24] G. Weihs, M. Reck, H. Weinfurter, and A. Zeilinger, Two-photon interference in optical fiber multiports, *Phys. Rev. A* **54**, 893 (1996).
- [25] A. Peruzzo, A. Laing, A. Politi, T. Rudolph, and J. L. O’Brien, Multimode quantum interference of photons in multiport integrated devices, *Nat. Commun.* **2**, 224 (2011).
- [26] N. Spagnolo, C. Vitelli, L. Aparo, P. Mataloni, F. Sciarrino, A. Crespi, R. Ramponi, and R. Osellame, Three-photon bosonic coalescence in an integrated tritter, *Nat. Commun.* **4**, 1606 (2013).

- [27] A. J. Menssen, A. E. Jones, B. J. Metcalf, M. C. Tichy, S. Barz, W. S. Kolthammer, and I. A. Walmsley, Distinguishability and many-particle interference, *Phys. Rev. Lett.* **118**, 153603 (2017).
- [28] M. Mirhosseini, O. S. Magaña-Loaiza, M. N. O’Sullivan, B. Rodenburg, M. Malik, M. P. J. Lavery, M. J. Padgett, D. J. Gauthier, and R. W. Boyd, High-dimensional quantum cryptography with twisted light, *New J. Phys.* **17**, 033033 (2015).
- [29] A. Babazadeh, M. Erhard, F. Wang, M. Malik, R. Nouroozi, M. Krenn, and A. Zeilinger, High-dimensional single-photon quantum gates: Concepts and experiments, *Phys. Rev. Lett.* **119**, 180510 (2017).
- [30] M. Kues, C. Reimer, P. Roztockı, L. R. Cortés, S. Sciara, B. Wetzell, Y. Zhang, A. Cino, S. T. Chu, B. E. Little, D. J. Moss, L. Caspani, J. Azaña, and R. Morandotti, On-chip generation of high-dimensional entangled quantum states and their coherent control, *Nature (London)* **546**, 622 (2017).
- [31] B. Brecht, D. V. Reddy, C. Silberhorn, and M. G. Raymer, Photon temporal modes: A complete framework for quantum information science, *Phys. Rev. X* **5**, 041017 (2015).
- [32] V. Ansari, J. M. Donohue, B. Brecht, and C. Silberhorn, Tailoring nonlinear processes for quantum optics with pulsed temporal-mode encodings, *Optica* **5**, 534 (2018).
- [33] S. De, V. Ansari, J. Sperling, S. Barkhofen, B. Brecht, and C. Silberhorn, Realization of high-fidelity unitary operations on up to 64 frequency bins, [arXiv:2206.06059](https://arxiv.org/abs/2206.06059).
- [34] L. Serino, J. Gil-Lopez, M. Stefszky, R. Ricken, C. Eigner, B. Brecht, and C. Silberhorn, Realization of a multi-output quantum pulse gate for decoding high-dimensional temporal modes of single-photon states, *PRX Quantum* **4**, 020306 (2023).
- [35] G. H. Golub and C. F. Van Loan, *Matrix Computations*, Johns Hopkins Studies in the Mathematical Sciences, 3rd ed. (Johns Hopkins University Press, Baltimore, 1996).